Electrochemical and Solid-State Letters, **8** (10) E67-E69 (2005)
1099-0062/2005/8(10)/E67/3/$7.00 © The Electrochemical Society, Inc.

Nonlinear Electrical Properties of Grain Boundaries in Oxygen Ion Conductors

Modeling the Varistor Behavior

René Meyer,[a,z] Xin Guo,[b,*] and Rainer Waser[a]

[a]*Institut für Festkörperforschung, Forschungszentrum Jülich, 52425 Jülich, Germany*
[b]*Department of Materials Science and Engineering, University of Florida, Gainesville, Florida 32611, USA*

We report on numerical simulations of the grain-boundary varistor behavior recently observed in Y_2O_3-doped CeO_2 of high purity. The aim of this study is to disclose the nature of the nonlinear electrical properties of the grain boundaries in oxygen ion conductors. Under small voltages (<25 mV), the simulation shows a linear current-voltage relation dominated by the grain-boundary resistance. Under intermediate voltages (25–200 mV), the simulation discloses a grain-boundary resistance breakdown and a nonlinear current-voltage relation. The increase of ionic charge carriers in the grain-boundary space-charge layer is the cause for the nonlinear behavior. Calculations are compared to experimental results.
 [DOI: 10.1149/1.2008940]

Manuscript received May 6, 2005. Available electronically August 4, 2005.

The specific grain-boundary conductivity of acceptor-doped ZrO_2 or CeO_2 is usually at least two orders of magnitude lower than that of the bulk,[1-8] depending on temperature and dopant level. When present, an intergranular impurity phase definitely contributes to the low grain-boundary conductivity,[1,2] however, in materials of high-purity the oxygen-vacancy depletion in the grain-boundary space-charge layer is the decisive cause of the low grain-boundary conductivity (space-charge depletion concept).[3-8] The space-charge depletion layer is formed by positively charged grain-boundary core states. Recently, electrical fields up to 2×10^5 V cm^{-1} were applied to the grain boundaries of 1.0 mol % Y_2O_3-doped CeO_2 at 400°C in air, and the grain-boundary properties were separated by means of impedance spectroscopy. It was discovered that the current-voltage relation for individual grain boundary is nonlinear (varistor behavior), which supports the space-charge depletion concept.[9] The use of raw materials of high purity in the sample preparation prevented the formation of a silicon-rich amorphous intergranular phase.

In this contribution, we present numerical simulation studies utilizing the back-to-back Schottky barrier model earlier developed for electronic conductors[10-16] to elucidate the nature of the grain-boundary varistor behavior in polycrystalline ionic conductors.

Model

The one-dimensional model space for the polycrystalline ion conductor consists of a single grain boundary, with the adjacency of two half grains. The width of the simulated model structure is 20 μm. Inside each grain, the concentration of oxygen vacancies is given by the amount of bulk acceptor states to maintain electroneutrality. Near the interface, oxygen vacancy depleted space-charge layers are formed due to the presence of positively charged donor-type grain boundary states. It is assumed that electrical conductivity of the grains and of the grain boundary space-charge layers exclusively results from the migration of oxygen vacancies. Vacancy mobility and dielectric constant are assumed to be constant all over the sample; the reduced grain boundary conductivity solely originates from a decreased concentration of oxygen vacancies in the space-charge layer. Free parameters of the model are grain size, acceptor concentration, oxygen vacancy mobility, dielectric constant, temperature, external voltage, and density of interface states. Grain size, acceptor concentration, temperature, and external voltage are chosen to meet the experimental conditions reported in Ref. 9. Oxygen vacancy mobility and dielectric constant used in the simulation were experimentally determined from the complex bulk impedance response. The only model parameter which cannot directly be determined from the experiment, is the concentration of interface states. However, the total conductivity serves as an indirect measure for the interface state density. In the simulation, the interface state density is varied under zero voltage conditions, until the calculated value of the dc conductivity was equal to the experimentally obtained total conductivity. To verify the space-charge approach, the total conductivity under dc bias predicted by model calculations was compared to the experimentally observed varistor behavior.

The ionic current and the concentration profile of oxygen vacancies as a function of external voltage result from the steady-state transport equation derived from the Nernst-Planck equation. The respective flux density j reads as

$$j = -D\frac{\partial[V_O^{\cdot\cdot}]}{\partial x} + \mu[V_O^{\cdot\cdot}]E \text{ with } \frac{\mu}{D} = \frac{|z|}{k_B T} \quad [1]$$

The steady-state solution of the transport equation is given by

$$\frac{\partial j}{\partial x} = -\frac{\partial[V_O^{\cdot\cdot}]}{\partial t} \equiv 0 \quad [2]$$

Here, D and μ terms are the diffusion coefficient and mobility (linked by the Nernst-Einstein equation), k_B is the Boltzmann constant, T denotes the temperature, and z is the charge number. From Eq. 1 and 2, the steady-state defect concentration can be calculated, if the local electric field E is known. This electric field can be calculated from

$$E(x) = \int_0^x \frac{\rho(\xi)}{\varepsilon_0 \varepsilon_r} d\xi + E_{ext} \quad [3]$$

The space-charge $\rho(x)$ reads as

$$\rho(x) = \begin{cases} Q_{IS} & \text{interface core} \\ e_0(2[V_O^{\cdot\cdot}](x) - N_A) & \text{space-charge layers} \\ 0 & \text{else} \end{cases} \quad [4]$$

N_A is the dopant concentration, e_0 denotes the elementary charge, and x and ξ denote the space position. Q_{IS} is the concentration of donor-type interface states situated at the grain boundary core. The concentration of oxygen vacancies in the grains serves as a further conditional equation to determine the model boundaries, which is given by $[V_O^{\cdot\cdot}] = 0.5N_A$.

An external voltage is taken into account by the difference of the electric potentials at the left and the right side of the simulation space. Here, electroneutrality is assumed even if an external voltage is applied. This is a good approximation for microcrystalline ceramics, but it might not be the case for nanocrystalline materials, where the interface space-charge layers of adjacent grain

* Electrochemical Society Active Member.
z E-mail: r.meyer@fz-juelich.de

Table I. Experimentally determined parameters and simulation results.

Simulation input[9]		
Acceptor concentration	5×10^{20} cm^{-3}	1 mol % Y_2O_3
Oxygen vacancy concentration	2.5×10^{20} cm^{-3}	
Grain size	~20 μm	
Mobility[a]	2.9×10^{-6} cm^2/Vs	From bulk conductivity
Diffusion coefficient[a]	8.3×10^{-8} cm^2/s	From Nernst-Einstein equation
Grain-boundary resistivity[a]	7.6×10^5 Ω cm	
Dielectric constant[a]	46	From bulk capacitance
Simulation output		
Potential barrier	0.39 eV	0.48 eV[7]
Grain-boundary state density	2×10^{14} e_0 cm^{-2}	
Inner electric field	3.6 MV/cm	

[a] at 400°C.

boundaries might overlap; more complicated boundary conditions for the defect concentration have to be applied for nanocrystalline materials.

The parameters determined from the previous experiments[9] are summarized in Table I, and were used as the simulation inputs. The charge of the grain-boundary core was estimated to be $Q_{IS} = 2 \times 10^{14}$ e_0 cm^{-2}. This core charge is required to cause a specific grain-boundary resistivity of 7.6×10^5 Ω cm, if no bias voltage is applied.

Results

Zero bias.— Figure 1 displays the distribution of oxygen vacancies in the space-charge layers, under the condition of zero external field. Due to the repulsive electrostatic force of the positive grain-boundary core charge, oxygen vacancies are depleted in the space-charge layers. The situation is very similar to the depletion of electrons in an n-type conductor, e.g., ZnO,[12,13] except for the fact that an ionic conductor is investigated here. The high concentration of uncompensated acceptors causes an inner electric field of 3.6 MV/cm in the center of the grain-boundary core. The potential barrier height is estimated at 0.39 eV by Poisson's equation, which is lower than the value of 0.48 eV calculated from an analytical approach.[7] The difference may result from the Schottky approximation used to describe the oxygen vacancy profile in the space-charge layer in the analytical solution.

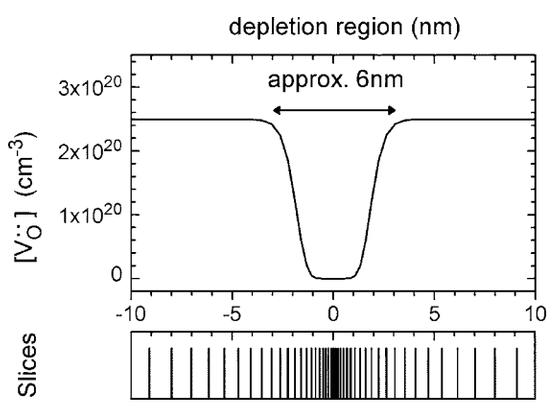

Figure 1. Upper graph: calculated depletion of oxygen vacancies and formation of space-charge layers due to a positive grain-boundary core charge. Lower graph: grid resolution of the finite differences approach at the grain boundary.

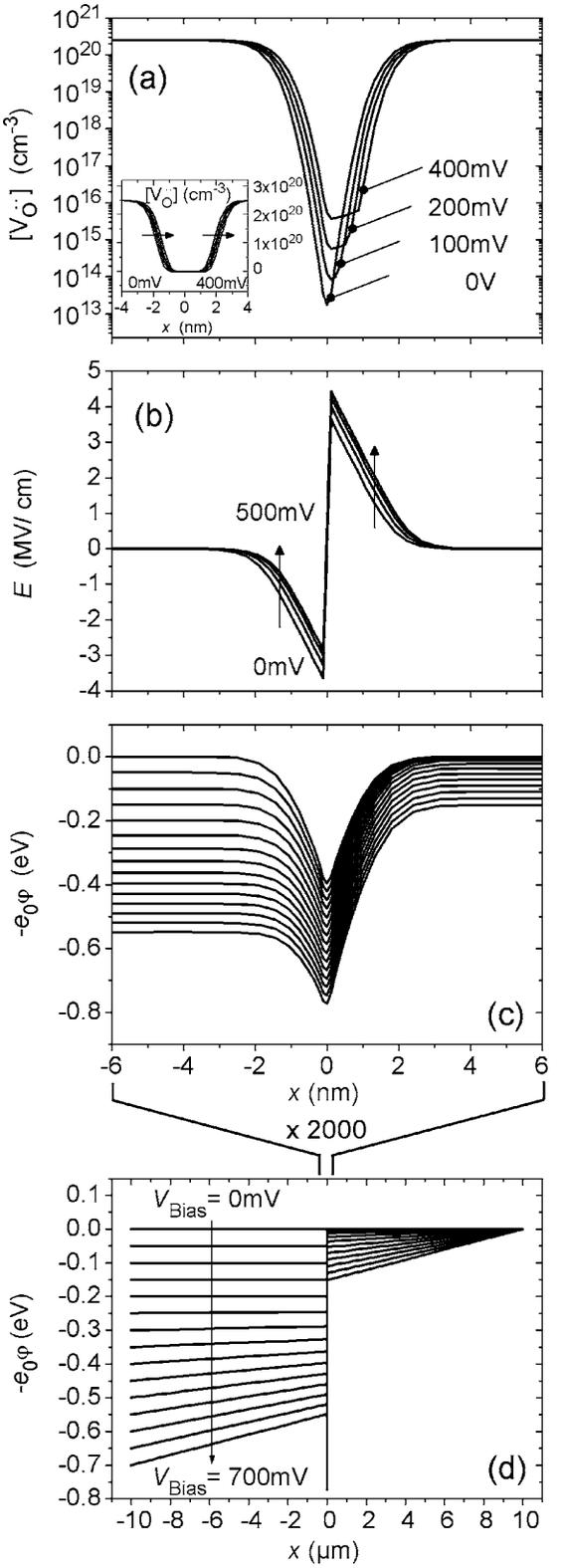

Figure 2. Redistribution of oxygen vacancies (a), inner electric field (b), and potential distribution across two grains separated by a grain boundary (d), and close to the grain boundary (c) in the presence of external electric fields.

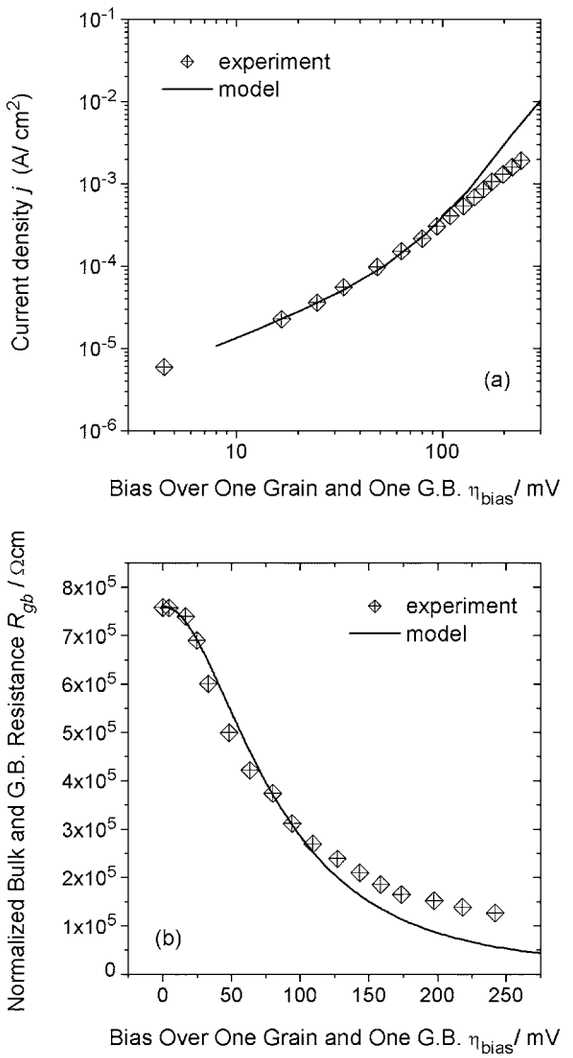

Figure 3. Varistor behavior of a single grain boundary obtained by experiment and by the simulation. In this figure, the grain-boundary resistance is normalized with A/L, with A being the cross-sectional area and L the thickness.

DC bias.— Under the effect of an external electric field, a redistribution of oxygen vacancies around the crystallographic grain boundary is disclosed by the simulation, as illustrated in Fig. 2a (inset in linear scale). On a logarithmic scale, a significant increase of the concentration of oxygen vacancies in the grain-boundary core is found, giving rise to a grain-boundary conductivity increase with increasing bias voltage. The inner electric field at the grain boundary under dc bias is shown in Fig. 2b. Here the external voltage induces an asymmetry with a slight increase of the field on the right side of the barrier, while the field is slightly decreased on the opposite side. The potential drop across the simulation space on the whole and close to the grain-boundary is displayed in Fig. 2c and d. In these figures, a small and a large signal behavior can be distinguished, when an external bias voltage is applied. For voltages smaller than 200 mV, most of the voltage drop falls across the space-charge layer. At higher voltages, a voltage drop over the grain is observed as well. Since the voltage drop directly correlates with the local conductivity, an increase of the grain-boundary conductivity is expected under high-field stress. This becomes clearer when we plot grain-boundary resistance and current density vs voltage.

Figure 3 illustrates the current voltage relation (a) and the grain-grain boundary resistance vs bias voltage (b) calculated from the steady-state solution for the ionic current as a function of the applied bias voltage; experimental data are also plotted for comparison. The simulation discloses a linear behavior for small bias voltages ($<$25 mV), as observed experimentally. At moderate voltages (25-200 mV), a nonlinear resistance decrease is found. For even higher voltages, the calculation yields a second linear regime, which is dominated by the bulk resistance, rather than the grain-boundary resistance. The second linear regime is not experimentally accessible due to the onset of the resistance degradation of the sample. The model and experiment show a quantitative agreement in the low-field region and the varistor region, as well as a semi-quantitative agreement at high fields. The differences in the high-field region might be due to a grain size distribution, or an inhomogeneous distribution of donor states at the grain-boundary core, giving rise to a local distribution of the grain-boundary potential. The latter might depend on the particular crystallographic orientation of adjacent grains, as reported for different small angle bicrystal grain boundaries in $SrTiO_3$,[17] which has not been considered in the simulation.

Conclusions

The dc response of a model grain boundary of an ionic conductor is calculated by a finite differences approach utilizing the back-to-back Schottky barrier model. A positive grain-boundary core charge leads to the lowering of the charge-carrier concentration in the space-charge layer. Therefore, the grain-boundary conductivity is significantly lower than the bulk value. Under a small bias voltage $<$25 mV, the resistance of the model is mainly dominated by the grain-boundary region, similar to the bias-free situation. The nonlinear current-voltage behavior at moderate voltages (25–200 mV) is found to originate from an increase of ionic charge carriers in the space-charge layer and the grain-boundary core. However, under an even higher voltage, the resistance is dominated by the bulk, rather than the grain boundary. In this case, the resistance current-voltage behavior becomes linear again.

It is demonstrated that the space-charge model gives a reasonable explanation for the grain-boundary varistor behavior of ionic conductors. Quantitative agreement between the experiment and the simulation strongly supports the space-charge model in acceptor-doped CeO_2 of high-purity.

Institut für Festkorperforschung assisted in meeting the publication costs of this article.

References

1. S. P. S. Badwal, *Solid State Ionics*, **76**, 67 (1995).
2. M. Gödickemeier, B. Michel, A. Orliukas, P. Bohac, K. Sasaki, L. Gauckler, H. Heinrich, P. Schwander, G. Kostorz, H. Hofmann, and O. Frei, *J. Mater. Res.*, **9**, 1228 (1994).
3. M. J. Verkerk, B. J. Middelhuis, and A. J. Burggraaf, *Solid State Ionics*, **6**, 159 (1982).
4. L. Heyne, in *Mass Transport in Solids*, E. Beniere and C. R. A. Catlow, Editors, p. 425, Plenum Press, (1983).
5. D. Bingham, P. W. Tasker, and A. N. Cormack, *Philos. Mag. A*, **60**, 1 (1989).
6. X. Guo and J. Maier, *J. Electrochem. Soc.*, **148**, E121 (2001).
7. X. Guo, W. Sigle, and J. Maier, *J. Am. Ceram. Soc.*, **86**, 77 (2003).
8. X. Guo and R. Waser, *Solid State Ionics*, **173**, 63 (2004).
9. X. Guo, S. Mi, and R. Waser, *Electrochem. Solid-State Lett.*, **8**, J1 (2005).
10. G. E. Pike and C. H. Seager, *J. Appl. Phys.*, **50**, 3414 (1979).
11. G. E. Pike and C. H. Seager, *Adv. Ceram.*, **1**, 53 (1989).
12. G. Blatter and F. Greuter, *Phys. Rev. B*, **33**, 3952 (1984).
13. F. Greuter and G. Blatter, *Semicond. Sci. Technol.*, **5**, 111 (1990).
14. R. Hagenbeck, L. Schneider-Störmann, M. Vollmann, and R. Waser, *Mater. Sci. Eng., B*, **39**, 179 (1996).
15. W. Heywang, *Solid-State Electron.*, **3**, 51 (1961).
16. R. Meyer and R. Waser, *Sens. Actuators B*, **101**, 335 (2004).
17. R. A. De Souza, J. Fleig, J. Maier, O. Kienzle, Z. Zhang, W. Sigle, and M. Ruhle, *J. Am. Ceram. Soc.*, **86**, 922 (2003).